Interplay between External Strain and Oxygen Vacancies on a Rutile $TiO_2(110)$ Surface

Da-Jun Shu,[*,+] Shu-Ting Ge, Mu Wang,[*,‡] and Nai-Ben Ming

National Laboratory of Solid State Microstructures and Department of Physics, Nanjing University, Nanjing 210093, China

(Received 25 April 2008; revised manuscript received 9 July 2008; published 12 September 2008)

Comprehensive first-principle calculations on strained rutile $TiO_2(110)$ indicate that the formation energy of different types of oxygen vacancies depends on the external strain. For the unstrained state, the energetically favorable oxygen vacancy (EFOV) appears on the bridging site of the first layer; when 3% tensile strain along $[1\bar{1}0]$ is applied, EFOV moves to the in-plane site, while 2% compressive strain along either [001] or $[1\bar{1}0]$ shifts EFOV to the subbridging site. We therefore suggest that the distribution of oxygen vacancies can be engineered by external strain, which may help to improve the applications of a TiO_2 surface where oxygen vacancy plays an important role.

DOI: 10.1103/PhysRevLett.101.116102 PACS numbers: 68.47.Gh, 68.35.Dv, 68.35.Gy, 68.35.Md

The most common defects on surfaces of transition metal oxides are oxygen vacancies, which play critical roles in applications such as heterogeneous catalysis, photoelectrolysis, biocompatibility, etc. [1–5]. If the nature and distribution of the oxygen vacancies can be controlled, the surface properties will then be modified for different applications. For this purpose, one needs to understand both the influence of oxygen vacancies on the surface properties and the responses of oxygen vacancies to different external fields [6,7].

External strain is unavoidable especially in the fabrication of nanostructures and thin films [8–10]. The responses of a nanostructure to the external strain are determined by its surface mechanical properties, which are strongly influenced by the surface defects [11–14]. For instance, it has recently been proposed that stress induced by absorption of atoms on graphene nanoribbons can be so strong that it may fold the nanoribbons forming single-walled nanotubes [14]. Similarly, vacancies can also have important influences on the mechanical properties [15,16]. If the effect of oxygen vacancy on surface mechanical properties of oxide is type dependent, the externally applied elastic strain can influence the nature and distribution of the surface defects and can therefore have an effect on the surface properties and reactivity [17,18]. However, our understanding of defect-dependent surface elastic properties of transition metal oxides is very limited so far.

In this Letter we take rutile $TiO_2(110)$ as a model system to study the elastic response of oxygen vacancies of transition metal oxide. We find that external strain can be applied to tune the type of energetically favorable oxygen vacancy (EFOV). The EFOV occurs on the bridging sites in an unstrained state and changes to the in-plane sites when 3% tensile strain along $[1\bar{1}0]$ is applied, whereas it shifts to the subbridging ones when 2% compressive strain along either [001] or $[1\bar{1}0]$ is applied. We therefore suggest that the nature and distribution of oxygen vacancies and thus the surface properties can be controlled by external strain.

The interaction of external strain and oxygen vacancies is attributed to the dependence of surface elastic properties of rutile $TiO_2(110)$ on the type of oxygen vacancy. Surface stress tensor $\sigma_{\alpha\beta}$ and surface elastic constants $S_{\alpha\beta\alpha'\beta'}$ can be expressed as [19,20]

$$\sigma_{\alpha\beta} = \frac{1}{A_L}\frac{\partial(A_L\gamma_L)}{\partial\epsilon_{\alpha\beta}} = \frac{\partial\gamma_L}{\partial\epsilon_{\alpha\beta}},$$
$$S_{\alpha\beta\alpha'\beta'} = \frac{\partial\sigma_{\alpha\beta}}{\partial\epsilon_{\alpha'\beta'}} = \frac{\partial^2\gamma_L}{\partial\epsilon_{\alpha\beta}\partial\epsilon_{\alpha'\beta'}}. \quad (1)$$

A_L is the area of the surface in an unstrained state, and γ_L is the Lagrangian surface energy per unit area in an unstrained state. The indices denote the two directions along the surface. To investigate the interplay between external strain and oxygen vacancies, we compare the surface energy of the stoichiometric surface and the defective surface with variation of external strain, from which the changes of vacancy formation energy and the surface elasticity are analyzed.

The calculations are based on density functional theory in the PW91 generalized gradient approximation [21],

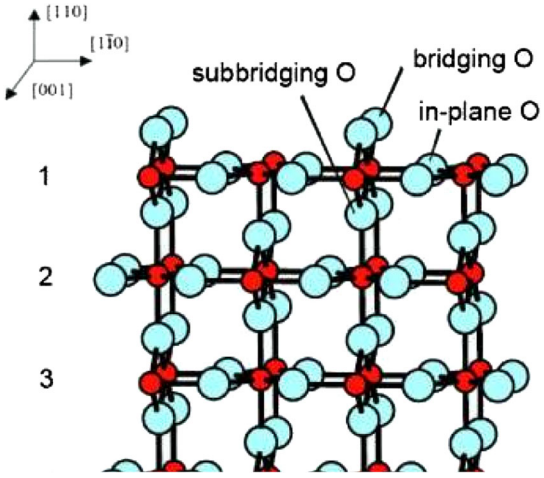

FIG. 1 (color online). Schematic of the rutile $TiO_2(110)$ surface. Large light spheres and small dark spheres stand for O and Ti atoms, respectively. The numbers on the left denote the trilayer number for further reference.

using the Vienna *ab initio* simulation package (VASP) code with projector augmented wave pseudopotentials [22]. An energy cutoff of 396 eV is used for expanding the Kohn-Sham wave functions. The rutile $TiO_2(110)$ surface is modeled as a (2×2) supercell consisting of a six-trilayer slab and a vacuum with thickness of five trilayers. The corresponding bulk structure is modeled by the same supercell except with no vacuum layers. A Monkhorst-Pack k-points grid [23] is $4 \times 8 \times 4$ for bulk structure and $2 \times 4 \times 1$ for the surface, which have been tested to be well converged. The bottom two trilayers are fixed to mimic the bulk, and the relaxation is carried out until all forces on the free ions are converged to 0.01 eV/Å. The stoichiometric rutile $TiO_2(110)$ surface is characterized by rows of bridging oxygen atoms along the [001] direction, between which is a trough consisting of two rows of in-plane oxygen atoms [24], as shown in Fig. 1.

We begin with the elastic response of an ideal stoichiometric $TiO_2(110)$ surface. Two configurations are used in order to check the relaxation effect on the surface elasticity: one is the unrelaxed slab, the other is the slab with a free surface while fixing the bottom two trilayers to mimic the bulk. The total energies of the supercell with relaxed and unrelaxed surfaces, E_{st} and E^u_{st}, respectively, as well as the total bulk energy E_b are calculated as a function of the applied strain along $[1\bar{1}0]$ and [001]. The surface energies of the unrelaxed surface (γ_u) and the relaxed surface (γ) are then calculated by

$$\gamma_u = (E^u_{\mathrm{st}} - E_b)/(2A_L), \quad \gamma = (E_{\mathrm{st}} - E_b)/A_L - \gamma_u. \quad (2)$$

The surface energy of the relaxed surface in the unstrained state is about 34 meV/Å^2(0.544 J/m^2), which is in agreement with the reported values [25,26]. The variation of surface energies with the strain along $[1\bar{1}0]$ is shown in Fig. 2. The surface stress and surface elastic constants in both the $[1\bar{1}0]$ and [001] directions of the ideal surface are calculated according to Eq. (1).

Surface relaxation of rutile TiO_2 affects surface elasticity significantly, as shown in Table I [part (a)]. Even the signs of σ and S of the relaxed surface are changed with respect to those of the unrelaxed surface, and so is the anisotropy of surface elasticity. Surface elastic constants in both directions become negative after relaxation, which means the surface is softer than its bulk counterpart. As for the anisotropy of surface elasticity, $(\sigma_{22} - \sigma_{11})$ changes from 10.53 to -53.62 and $(S_{2222} - S_{1111})$ changes from 13.89 to -36.08 after relaxation, all in units of eV/(1×1).

We now introduce oxygen vacancy (OV) in the outmost three trilayers, the OV density being $\theta = 1/4$ per unit cell. There are three types of oxygen atoms in each trilayer, termed as bridging, in-plane, and subbridging oxygen atoms [24], as marked in Fig. 1. Thus three types of OVs can be introduced correspondingly by removing different types of oxygen atoms. We distinguish the oxygen vacancies by prefixing the trilayer number to the oxygen types.

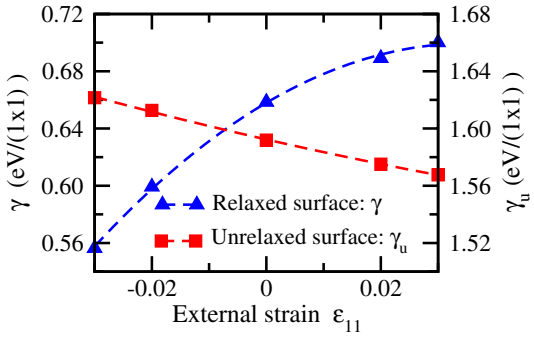

FIG. 2 (color online). The surface energy of relaxed surface (triangles) and unrelaxed one (squares) with variation of the applied strain. The dashed curves are quadratic fitted.

For example *2-in-plane OV* stands for the oxygen vacancy formed by removing an in-plane oxygen in the second trilayer. The supercell is fully relaxed while fixing the bottom two trilayers to mimic the bulk, and the vacancy formation energy can be expressed as

$$E_{\mathrm{OV}} = E_{\mathrm{vac}} - E_{\mathrm{st}} + \tfrac{1}{2}E_{\mathrm{O}_2}, \quad (3)$$

where E_{O_2} is the energy of an isolated O_2 molecule (which is -8.835 eV in our calculation). E_{st} and E_{vac} stand for the energy of the stoichiometric structure and that of the same structure except containing an OV, respectively.

The vacancy formation energy E_{OV} as a function of OV depth is shown in Fig. 3, where the depth is defined as the distance below the 1-bridging oxygen atoms of the unrelaxed perfect surface. It is clear that the 1-bridging OV is the most easily formed one due to its lowest formation energy, which is consistent with the experimental results [24]. Formation energies of in-plane OVs almost remain constant at different depths, which is close to that of a bulk OV [27,28]. The formation energies of the bridging and subbridging OVs appear in a kind of odd-even oscillation behavior, both of which tend to approach the formation energy of a bulk OV with increasing depth as previously reported [28,29].

TABLE I. (a) Surface energy and surface elasticity of unrelaxed and relaxed rutile $TiO_2(110)$ surfaces. (b) Changes of surface energy, surface stress and surface elasticity induced by different types of oxygen vacancies. The units are eV/(1×1). The subscripts 11 and 22 denote the directions along $[1\bar{1}0]$ and [001], respectively.

(a) Perfect surface	γ	σ_{11}	σ_{22}	S_{1111}	S_{2222}
Unrelaxed surface	1.60	−0.92	9.61	5.43	19.22
Relaxed surface	0.66	2.34	−51.28	−66.46	−102.54
(b) Oxygen vacancy	$\Delta\gamma$	$\Delta\sigma_{11}$	$\Delta\sigma_{22}$	ΔS_{1111}	ΔS_{2222}
1-bridging	2.17	0.51	−1.66	−2.42	−29.36
2-bridging	2.58	0.43	−0.88	−8.38	−12.66
1-in-plane	2.40	−5.02	−2.73	−151.01	−34.03
2-in-plane	2.44	−5.51	−2.95	−157.96	−39.62
1-subbridging	2.21	1.50	−0.63	−51.67	−62.98
2-subbridging	2.52	0.18	−0.41	−3.99	−81.19

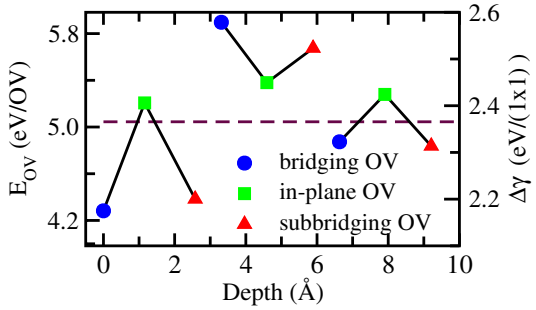

FIG. 3 (color online). The oxygen vacancy formation energy E_{OV} as a function of the OV depth, where the depth is defined as the distance below the unrelaxed 1-bridging O atoms. The dashed line denotes the bulk vacancy formation energy. Solid lines link the three types of OVs in each trilayer. On the right, we label the surface energy change induced by oxygen vacancy in the supercell.

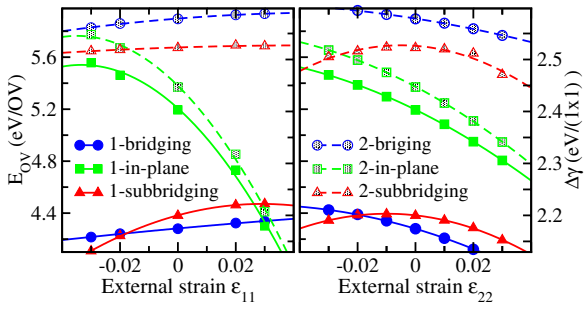

FIG. 4 (color online). The oxygen vacancy formation energy E_{OV} as a function of the applied strain along $[1\bar{1}0]$ and [001]. On the right, the surface energy change induced by oxygen vacancy in the supercell is labeled. The curves are quadratic fitted.

The formation energy of vacancies is verified using a (2×4) supercell ($\theta = 1/8$). The absolute values of the formation energies decrease by 0.88, 0.63, and 0.60 eV for 1-bridging, 1-in-plane, and 1-subbridging OV, respectively, which means that vacancies with lower density are easier to form [30]. However, the relative differences in the formation energy of different types of vacancies change little when defect density decreases. Therefore a (2×2) supercell is used to study the strain effect for the sake of computation efficiency.

Strain along $[1\bar{1}0]$ and [001] is now applied to the slab containing an OV in different sites. Atoms are relaxed while fixing the bottom two trilayers in their bulk counterparts. The formation energy of each type of OV in the outmost two trilayers is obtained according to Eq. (3) and shown in Fig. 4 as a function of the applied strain.

It is obvious that the OV formation energy can vary with the external strain, depending on the type of OVs and the direction along which the external strain is applied. The probability of forming an OV at different sites can be tuned accordingly by external strain. The bridging OV in the first trilayer is the energetically favorable oxygen vacancy under strain ϵ_{11} between -2% and 3% due to its lowest formation energy. When about 3% tensile strain is applied along $[1\bar{1}0]$, the in-plane OV becomes the EFOV. The EFOV site shifts to the subbridging one in the first layer when 2% compressive strain is applied along either direction.

Since it is known that OVs play important roles in surface processes in applications of TiO_2, our findings may help to understand the detailed surface activity with strain, and it should be possible to control the surface vacancy and thus the surface reactivity by using externally strain. In reality, vacancy distribution is also influenced by kinetic factors, since the diffusion barrier prevents the system from reaching the equilibrium distribution. The diffusion barrier of vacancies along the [001] direction (oxygen rows) is reported to be $E_d = 1.1$ eV, much smaller than the vacancy formation energy [31]. The diffusion barrier of vacancies along the direction normal to the surface is expected to be a little larger.

For realistic applications, the stability of stressed rutile should be considered. It is known that rutile is the thermodynamically stable phase in bulk, while it is less stable than the anatase phase when the size is decreased to a few nanometers [32]. Since external strain is usually applied to epitaxial layer via the substrate, the strained rutile is stable against transformation into anatase due to the large difference in structure parameters between rutile and anatase [24]. Meanwhile, the strained film remains coherent only when its thickness is smaller than a critical value $h_{cri} = 2(V_{ad} - 2\gamma)/k_b\epsilon^2$, where V_{ad} is the $TiO_2(110)$/substrate interface adhesion energy, γ is the surface energy, and k_b denotes the modulus of elasticity. A typical V_{ad} of 2 eV per unit cell leads to the critical thickness of 18 and 8 nm for 2% and 3% strain, respectively, which indicates that the strain range we consider here is experimentally accessible.

We are now able to understand the odd-even oscillation of the (sub)bridging OV formation energies shown in Fig. 3. As discussed previously, the sixfold coordinated Ti atoms (TA_{6c}) on the rutile $TiO_2(110)$ surface move upwards, whereas the fivefold coordinated Ti atoms (TA_{5c}) move downwards [24]. Considering the similarity between the $[1\bar{1}0]$ and [110] directions, the effect of the upward relaxation of TA_{6c} atoms on the (sub)bridging OV formation energy in odd trilayers is equivalent to that of tensile strain along $[1\bar{1}0]$ on the in-plane oxygen vacancies. Therefore the (sub)bridging OV formation energy in odd trilayers is smaller than that in the bulk phase according to Fig. 4. Similarly, the effect of the downward relaxation of the TA_{5c} atoms on the formation energy of (sub)bridging oxygen atoms in the even trilayers is equivalent to that of compressive strain on the in-plane OVs, which makes the (sub)bridging OV higher than that in the bulk. The consistency between the effect of externally applied strain and that of surface relaxation induced local strain further supports our original idea that external strain can be used to control the OV formation and distribution.

To get the influence of oxygen vacancies on the surface elasticity, we label the vacancy-induced change of surface

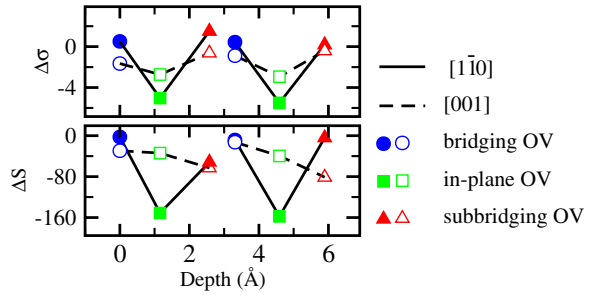

FIG. 5 (color online). The changes of the surface stress and surface elastic constants induced by the OV as a function of the OV depth, where the depth is defined as the distance below the unrelaxed 1-bridging O atoms. Lines are used to guide the three OVs in the same trilayer. $\Delta\sigma$ and ΔS are in units of eV/(1 × 1).

energy $\Delta\gamma$ on the right of vertical axis in Fig. 4, which is calculated as

$$\Delta\gamma = \frac{E_{\mathrm{vac}} - E_{\mathrm{st}}}{A_L} \equiv \theta \frac{E_{\mathrm{OV}} - \frac{1}{2}E_{O_2}}{A_{L0}}, \qquad (4)$$

where θ is the density of vacancies and A_{L0} is the area per unit cell. The data of the vacancy-induced changes of surface stress $\Delta\sigma$ and surface elastic constants ΔS are thus obtained according to Eq. (1). Values of $\Delta\gamma$, $\Delta\sigma$, and ΔS are proportional to OV density even when the density dependence of E_{OV} is ignorable, as suggested in Eq. (4). The depth dependent $\Delta\sigma$ and ΔS for $\theta = 1/4$ are shown in Fig. 5, and the value of $\Delta\gamma$, $\Delta\sigma$, and ΔS induced by oxygen vacancies are listed in Table I [part (b)].

It is shown that the decrease of the elastic constants in [1$\bar{1}$0] induced by in-plane OVs is the most obvious. Since compressive stress is also induced in this direction, the formation energy of in-plane OVs decreases rapidly with increasing strain along [1$\bar{1}$0] and becomes the lowest under 3% tensile strain. Under compressive strain, formation energy of the subbridging OV becomes the lowest. It is because of this that the subbridging OV induces more tensile stress in [1$\bar{1}$0] and less compressive stress in [001] as well as smaller elastic constants in both directions than the bridging one does. It is generally accepted that the influences of OVs on the surface mechanical properties of oxides depend on the OV types as well as the metal elements. One can therefore expect a similar reverse trend of vacancy formation for other metal oxides, for instance, the alkaline-earth oxides, where in normal state OV formation energies decrease along the alkaline-earth series and in going from bulk to the surface [33].

In conclusion, we demonstrate here that the formation energy of various types of OVs on the surface of rutile TiO_2(110) depends on external strain. For the unstained state, EFOV appears on the bridging site of the first layer; when 3% tensile strain along [1$\bar{1}$0] is applied, EFOV moves to the in-plane site, while when 2% compressive strain along either [001] or [1$\bar{1}$0] is applied, EFOV favors the 1-subbridging site instead. This effect originated from the different elastic responses of the OVs at different sites, which implies a universal approach to control the distribution of OVs via external strain field.

The numerical calculations have been carried out at the Shanghai Supercomputer Center. The authors acknowledge support from the Ministry of Science and Technology of China (2004CB619005, 2006CB0L1004).

*Corresponding author.
+djshu@nju.edu.cn
‡muwang@nju.edu.cn

[1] R. Asahi *et al.*, Science **293**, 269 (2001).
[2] R. Schaub *et al.*, Phys. Rev. Lett. **87**, 266104 (2001).
[3] E. Wahlstrom *et al.*, Phys. Rev. Lett. **90**, 026101 (2003).
[4] O. Bikondoa *et al.*, Nature Mater. **5**, 189 (2006).
[5] Y. Han *et al.*, J. Phys. Chem. C **111**, 16 397 (2007).
[6] D. O. Klenov *et al.*, Appl. Phys. Lett. **82**, 3427 (2003).
[7] H. Kamisaka and K. Yamashita, Surf. Sci. **601**, 4824 (2007).
[8] D. J. Shu, F. Liu, and X. G. Gong, Phys. Rev. B **64**, 245410 (2001).
[9] B. Yang, F. Liu, and M. G. Lagally, Phys. Rev. Lett. **92**, 025502 (2004).
[10] G. H. Lu, M. Cuma, and F. Liu, Phys. Rev. B **72**, 125415 (2005).
[11] G.-F. Wang and X.-Q. Feng, Appl. Phys. Lett. **90**, 231904 (2007).
[12] Q. Lu and B. Bhattacharya, Nanotechnology **16**, 555 (2005).
[13] C. W. Pao, D. J. Srolovitz, and C. V. Thompson, Phys. Rev. B **74**, 155437 (2006).
[14] D. Yu and F. Liu, Nano Lett. **7**, 3046 (2007).
[15] S.-H. Jhi *et al.*, Phys. Rev. Lett. **86**, 3348 (2001).
[16] C.-S. Shin *et al.*, J. Appl. Phys. **93**, 6025 (2003).
[17] T. Shibata *et al.*, J. Phys. Chem. B **107**, 10 696 (2003).
[18] P. Müller and A. Saúl, Surf. Sci. Rep. **54**, 157 (2004).
[19] V. B. Shenoy, Phys. Rev. B **71**, 094104 (2005).
[20] M. Schmid *et al.*, Phys. Rev. B **51**, 10 937 (1995).
[21] J. P. Perdew, K. Burke, and M. Ernzerhof, Phys. Rev. Lett. **77**, 3865 (1996).
[22] P. E. Blöchl, Phys. Rev. B **50**, 17 953 (1994); G. Kresse and D. Joubert, Phys. Rev. B **59**, 1758 (1999).
[23] H. Monkhorst and J. Pack, Phys. Rev. B **13**, 5188 (1976).
[24] U. Diebold, Surf. Sci. Rep. **48**, 53 (2003).
[25] J. Oviedo, M. Miguel, and J. Sanz, J. Chem. Phys. **121**, 7427 (2004).
[26] S. H. Overbury, P. A. Bertrand, and G. A. Somorjai, Chem. Rev. **75**, 547 (1975).
[27] K. S. Forland, Acta Chem. Scand. **18**, 1267 (1964).
[28] K. Hameeuw *et al.*, Phys. Status Solidi A **203**, 2219 (2006).
[29] T. Bredow *et al.*, Phys. Rev. B **70**, 035419 (2004).
[30] M. V. Ganduglia-Pirovano, A. Hofmann, and J. Sauer, Surf. Sci. Rep. **62**, 219 (2007).
[31] Z. Zhang *et al.*, Phys. Rev. Lett. **99**, 126105 (2007).
[32] H. Zhang and J. F. Banfield, J. Mater. Chem. **8**, 2073 (1998).
[33] J. Carrasco, N. Lopez, F. Illas, and H.-J. Freund, J. Chem. Phys. **125**, 074711 (2006).